Single-cell RNA-seq necroptosis-related genes predict the prognosis of breast cancer and affect the differentiation of CD4+ T cells in tumor immune microenvironment

LI GUO[1*], XIUZHEN MA[2*], HONG LI[2], SHUXUN YAN[1], KAI ZHANG[1] and JINPING LI[2]

[1]Clinical Medical College of Ningxia Medical University, Yinchuan, Ningxia Hui Autonomous Region 750003, P.R. China; [2]Department of Surgical Oncology, General Hospital of Ningxia Medical University, Yinchuan, Ningxia Hui Autonomous Region 750004, P.R. China

Received February 8, 2024; Accepted April 30, 2024

DOI: 10.3892/mco.2024.2747

Abstract. Breast cancer (BC) is one of the most prevalent types of malignancy and a major cause of cancer-related death. The purpose of the present study was to identify prognostic models of necroptosis-related genes (NRGs) in BC at the single-cell RNA-sequencing level and reveal the role of NRGs in tumour immune microenvironment (TIME). A risk model was constructed based on Cox regression and LASSO methods. Next, high-scoring cell populations were searched through AUCell scores, and cell subtypes were then analyzed by pseudotime analysis. Finally, the expression level of the model genes was verified by reverse transcription-quantitative (RT-qPCR). A new prognostic model was constructed and validated based on five NRGs (BCL2, BIRC3, AIFM1, IFNG and VDAC1), which could effectively predict the prognosis of patients with BC. NRGs were found to be highly active in CD4+ T cells and differentially expressed in their developmental trajectories. Finally, the RT-qPCR results showed that most of the model genes were significantly overexpressed in MDA-MB-231 and MCF-7 cells ($P<0.05$). In conclusion, an NRG signature with excellent predictive properties in prognosis and TIME was successfully established. Moreover, NRGs were involved in the differentiation and development of CD4+ T cells in TIME. These findings provide potential therapeutic strategies for BC.

Correspondence to: Professor Jinping Li, Department of Surgical Oncology, General Hospital of Ningxia Medical University, 804 Shengli Street, Xingqing, Ningxia Hui Autonomous Region 750004, P.R. China
E-mail: 2634497264@qq.com

*Contributed equally

Key words: breast cancer, single-cell RNA sequencing, necroptosis, prognosis

Introduction

Breast cancer (BC) is currently the most prevalent cancer and the leading cause of cancer death in women, accounting for 25% of all cancers and 15% of cancer deaths worldwide (1). The main factor leading to the difficulty of treatment is the high heterogeneity of BC, which is susceptible to relapse and metastasis (2). At present, it is mainly based on the TNM stage and estrogen receptor (ER), progesterone receptor (PR) and human epidermal growth factor receptor 2 (HER2) to predict the prognosis of BC and guide treatment. However, patients with the same molecular subtypes have different responses to treatment, resulting in different outcomes (3,4). Therefore, further searching for molecular therapeutic targets of BC and constructing its prognostic model have become the focus of research.

Necroptosis is a new form of programmed necrotic cell death, which is similar to apoptosis in mechanism and necrosis in morphology (5). When necroptosis occurs, the cell membrane breaks and the cell contents are released, which leads to a severe inflammatory response that does not depend on caspase (6,7). Necroptosis is regulated by the receptor interacting protein kinase 3 (RIPK3) and the mixed lineage kinase domain-like (MLKL) pseudokinase (8). Emerging data indicated that necroptosis plays a considerable role in tumorigenesis, tumor progression and regulation of tumor immunity (9). In the past decade, necroptosis has been studied in a variety of cancers, most of which show low expression of RIPK3 or MLKL in tumors, which is related to short survival time and poor prognosis (10,11). It has been reported that necrotic apoptosis is the main form of tumor cell death in mouse BC model (12). Therefore, inducing necroptosis of BC cells can become a new and promising therapeutic strategy for BC.

Immunotherapy for cancer has changed the course of cancer treatment (13). Although immunotherapy for BC helps to improve the overall survival (OS) rate of patients, the current response rate of immunotherapy (such as checkpoint blocking) is only 10-30% (14). Therefore, it is necessary to find a new way of immunotherapy for BC. In tumor microenvironment (TME), necroptosis can increase tumor antigen load, enhance antitumor immunity, and cooperate with immune checkpoint

blocking to promote lasting tumor clearance (15). However, there is significant intratumoral heterogeneity in immune cell infiltration (16). A recent study has shown that single-cell RNA-sequencing (RNA-seq) technology plays an important role in analyzing the immunosuppressive microenvironment of metastatic BC (17). Therefore, identifying BC immune cell subpopulations at the single-cell level and exploring the expression of necroptosis genes will contribute to the immunotherapy of BC.

In the present study, it was aimed to comprehensively analyze the expression pattern of necroptosis related-genes (NRGs) in BC, construct NRGs' signature to predict the prognosis of patients with BC, and explore the relationship between necroptosis and BC tumour immune microenvironment (TIME) at the single-cell level. It was found that NRGs were highly active in $CD4^+$ T cells and differentially expressed in their developmental trajectories. Then, based on NRGs, three necroptosis-associated subtypes that could also differentiate patient outcomes were found. Next, a new prognostic model based on NRGs, which could effectively predict the prognosis of patients with BC, was constructed and validated. Finally, the prognostic genes were analyzed from the perspectives of immune checkpoints, immune cell infiltration and somatic mutations, revealing that they could serve as a novel potential BC prognostic biomarker.

Materials and methods

Data acquisition and processing. The BC related single-cell dataset GSE114724 was downloaded from the GEO database (https://www.ncbi.nlm.nih.gov/geo/) through the GEOquery package. The data source is *Homo sapiens*, and its data platform is GPL16791. A total of three BC samples were selected for follow-up analysis: GSM3148575, GSM3148577 and GSM3148578. Sample GSM3148575 included 7,096 cells, sample GSM3148577 included 4,926 cells and sample GSM3148577 included 5,232 cells.

In the present study, R packet 'Seurat' (18) was used to create single-cell data as Seurat objects, and the proportion of mitochondria in each cell was calculated by the 'PercentageFeatureSet' function of Seurat package. Low-quality cells were excluded based on three quality measures: Mitochondrial gene content >5%, feature <500, and unique molecular identifier (UMI) count >20,000. After the aforementioned steps, 10,261 cells were obtained.

Subsequently, the samples were integrated and the Canonical Correlation Analysis (CCA) method was used to remove the batch effect. For Seurat objects, linear dimensionality reduction was performed and the most variable genes expressed in the dataset were used to calculate principal component (PC). Then, the 'FindNeighbors' and 'FindClusters' functions of Seurat were used to group the cells into the optimal number of cluster in order to identify the cell types, and Uniform Manifold Approximation and Projection (UMAP) was used to reduce the information captured in the selected important PCs to two dimensions, and the visual clustering of cells was realized based on graphics.

BC transcriptome data was downloaded from The Cancer Genome Atlas Genomic Data Commons (TCGA GDC) official website (https://portal.gdc.cancer.gov/), and the selected data type was Fragments Per Kilobase Million. And the clinical data of patients with BC were downloaded from the TCGA GDC website (n=1,285). After removing samples that lacked clinical information, TCGA-BC included 878 BC samples and 41 paracancerous tissue samples. Details of patients with BC are listed in Table I.

In addition, the BC dataset GSE42568 was downloaded from the GEO database through the GEOquery package to verify the accuracy of the prognostic model. The GSE42568 (19) data set comes from *Homo sapiens*, and its data platform is GPL570. It contains a total of 121 samples, including 104 cases of BC and 17 cases of normal samples. BC samples were selected from these samples for survival analysis.

In the present study, NRGs were obtained from previous literature for follow-up analysis, including 101 NRGs (Table SI) (20). At the same time, the immune checkpoint genes (ICGs) were obtained from the previous literature for follow-up analysis; a total of 47 ICGs were obtained (Table SII) (21). To analyze somatic mutations in TCGA patients with BC, 'TCGAbiolinks' R package was used to download the patient's 'Masked Copy Number Segment' data (n=897).

Cell annotation. A total of 14 clusters were visualized by UMAP, and 7 different cell types were revealed by artificial annotation of cell type marker genes, including B cells, $CD4^+$ T cell, $CD8^+$ T cell, progenitor cells, endothelial cells, natural killer (NK) T cells and regulatory T cells. Cell group marker genes were displayed in Table II. In order to understand the expression pattern of diagnostic markers in patients with BC, the differences of gene expression were compared in different cell groups.

Identification of differential genes in cell groups. For the seven cell groups that had been annotated, the function 'FindAllMarkers' was used to calculate the differential genes among all cell groups, and the genes selected according to the criteria of |log2FoldChange|>0.25 and P<0.05 were used as the single-cell differentially expressed genes (scDEGs) for further study. Then, NRGs and scDEGs were intersected, and the obtained genes were used as the key genes in the present study.

Using AUCell to score the cell populations. AUCell could identify cells with active gene sets in single-cell RNA-seq data. AUCell used 'Area Under Curve' (AUC) to calculate whether the key subset of the input gene set was enriched in the expressed genes of each cell. Key genes for AUCell scoring were selected and high-scoring cell populations were searched.

Gene Ontology (GO) and Kyoto Encyclopedia of Genome and Genomes (KEGG) pathway functional enrichment analysis. The differential genes in $CD4^+$ T cell population were analyzed by GO annotation and KEGG pathway enrichment analysis using 'clusterProfiler' package of R, and the critical value of FDR <0.05 was considered to be statistically significant. The first 8 results with the lowest P-value of biological processes (BP), cellular components (CC) and molecular functions (MF) in GO and the top 10 results with the lowest P-value of KEGG were shown in bar chart and bubble chart, respectively.

Table I. TCGA-breast cancer sample baseline data in TCGA database.

Characteristics	Number of cases (%)
T stage	
T1	236 (27)
T2	515 (59)
T3	97 (11)
T4	30 (3)
N stage	
N0	429 (49)
N1	299 (34)
N2	96 (11)
N3	54 (6)
M stage	
M0	860 (98)
M1	18 (2)
Overall survival	
Dead	130 (15)
Alive	748 (85)
Sex	
Female	867 (99)
Male	11 (1)

TCGA, The Cancer Genome Atlas.

Table II. Cell population marker gene information.

Cluster/subsets	Cells (N)	Marker gene
$CD8^+$ T cells	2804	GZMK, CD8A, KRT86
$CD4^+$ T cells	1337	IL7R, CCR7
B cells	1720	KLF2, SELL
Progenitor cells	81	MCM7, TUBA1B
Endothelial cells	30	STMN1, HMGN2
Regulatory T cells	1647	IL2RA, FOXP3
Natural killer T cells	2642	ZNF683, MT-ND6

Pseudotime analysis. Pseudotime analysis could arrange each cell on the corresponding track according to the time sequence gene expression, and divide the sample into several differentiated cell groups according to the gene expression status to generate an intuitive tree map of pedigree development, which could predict the differentiation and development trajectory of cells. For the subsets of $CD4^+$ T cells, pseudotime analysis was used to predict the differentiation and development of subsets, and the changes of NRGs during the pseudotime process were analyzed.

Disease typing based on key genes. Consistent clustering is a method that could determine the number and members of possible clusters in a dataset. The R-packet 'ConsensusClusterPlus' was used to cluster the TCGA-BC dataset consistently using the aforementioned key genes in order to improve distinguishing different subtypes of BC. In addition, PC analysis (PCA) was used to analyze different BC molecular subtypes.

Construction of prognostic risk model based on key genes. In order to determine the effect of key genes on the prognosis of patients with BC, the Least Absolute Shrinkage and Selection Operator (LASSO) algorithm was used to construct the prognostic risk model of BC. The 'glmnet' package of R was used to select the LASSO feature genes. The selected features were screened in the process of model construction, and the genes in the best model were selected as the BC prognostic genes. Finally, according to the risk regression coefficients of all genes in the model, a formula for calculating the risk score was constructed:

$$\text{riskScore} = \sum_i \text{Coefficient (hub gene}_i) * \text{mRNA Expression (hub gene}_i)$$

In the present study, a prognostic risk model for BC samples was constructed from TCGA datasets, and R-packet 'maxstat' was used to calculate the best cut-off value of the ability to predict the survival time of patients with BC. Based on cut-off value, the patients were divided into high- and low-risk groups. The Kaplan-Meier (KM) method of R-packet 'survival' was used for survival analysis, and R-packet 'survminer' was used to visualize the results. In addition, GEO datasets were used to validate the prognostic model.

Evaluation model of prognostic risk model. Based on the TCGA-BC dataset, univariate and multivariate COX regression analysis was used to evaluate the ability of risk scores combined with clinicopathological features of patients with BC to predict OS, and the results were shown through forest maps. In addition, according to the clinical information of the sample in the present study, R-packet 'rms' was used to construct a line chart to study the relationship between clinical factors and prognosis, and the calibration curves of 1-, 3- and 5-year, respectively, were drawn.

Immune infiltration analysis. CIBERSORT (22) calculation method was used to analyze the data of high- and low-risk groups in TCGA-BC dataset to obtain immune infiltration information, and R 'ggplot2' package was used to draw a bar chart to show the distribution of 22 kinds of immune cell infiltration in each sample. Subsequently, a heat map was drawn to reflect the correlation between prognostic genes and immune cells. Finally, the scores of different immune cells were compared between high- and low-risk groups, so as to obtain immune cells with different infiltration levels between the two groups.

In the study of Ru *et al* (23), the data of 28 kinds of immune cells were collected, R-packet Gene Set Variation Analysis was used to explore the difference of immune infiltration among different BC molecular subtypes, and the results were shown by box chart.

Estimate. In the present study, Estimate R package was used to estimate the proportion of immune components and stromal components of each sample in TME in the form of ImmuneScore, StromalScore and ESTIMATEScore. The

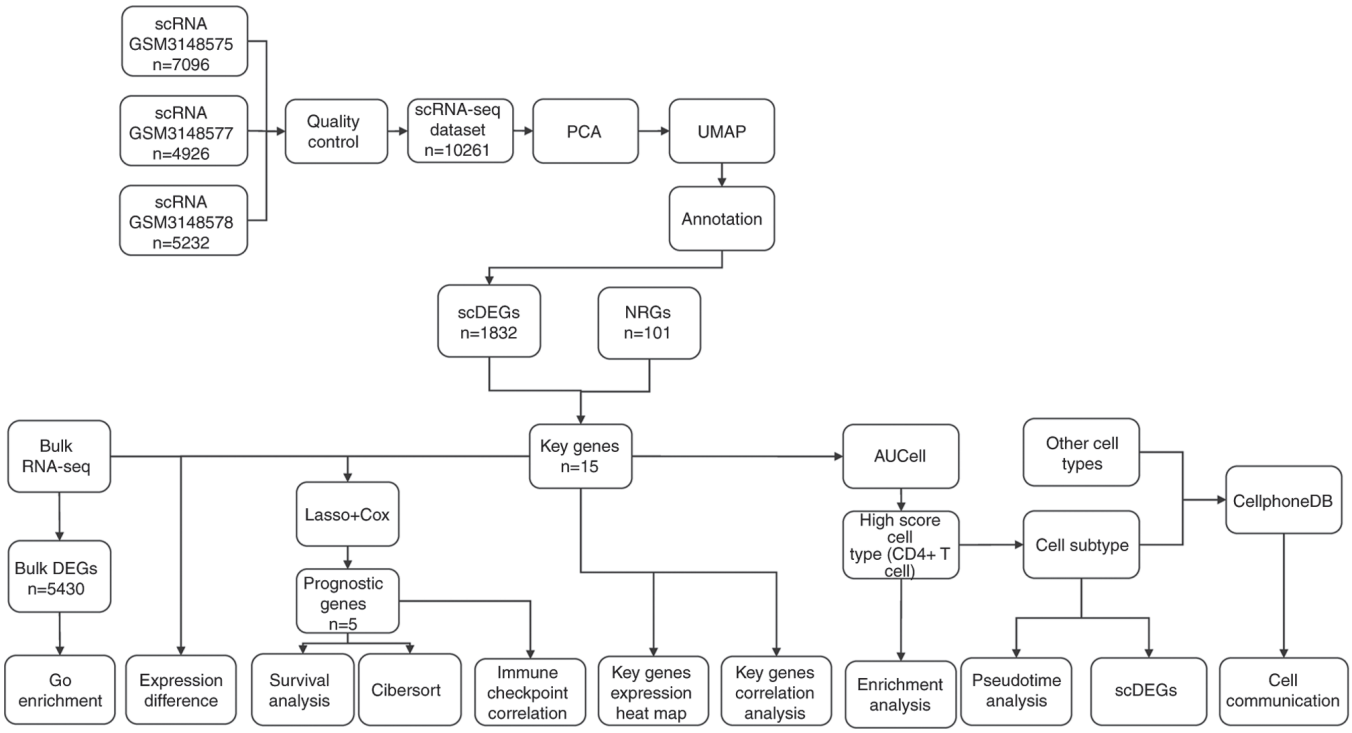

Figure 1. Overall analysis flowchart. PCA, principal component analysis; UMAP, uniform manifold approximation and projection; NRGs, necroptosis-related genes; scDEGs, single-cell differentially expressed genes; GO, Gene Ontology.

higher the score, the greater the proportion of corresponding components in TME.

Analysis of somatic mutation and differential expression of HLA gene family. R-packet 'maftools' was used to visualize somatic mutations in high- and low-risk groups in TCGA-BC datasets, and the mutation differences between the two groups were compared; the results were shown in the waterfall map. At the same time, the differential expression of human leukocyte antigen (HLA) family genes was analyzed in high- and low-risk groups.

Cell culture. The MDA-MB-231 cell line (CL-0150, Procell Life Science & Technology Co., Ltd.) was cultured at 37˚C with 5% CO_2 in DMEM (cat. no. PM150210; Procell Life Science & Technology Co., Ltd.) with 10% fetal bovine serum (FBS) (cat. no. 10091148; Gibco; Thermo Fisher Scientific, Inc.), 100 μg/ml streptomycin and 100 U/ml penicillin (cat. no. SV30010; Hyclone; Cytiva). The MCF10A cell line (cat. no. CRL-10317; Shanghai Zhong Qiao Xin Zhou Biotechnology Co., Ltd.) was cultured in 37˚C, 5% CO_2, complete medium (cat. no. ZQ-1311; Shanghai Zhong Qiao Xin Zhou Biotechnology Co., Ltd.) containing 5% horse serum and 1% penicillin/streptomycin (Hyclone; Cytiva). MCF-7 cells were borrowed from Key Laboratory of Fertility maintenance, Ministry of Education (Professor Jing Chen). However, appropriate measures were received to ensure that the source and quality of these cells were reliable, and these cells were used for the present research to explore some of the characteristics of BC.

Reverse transcription-quantitative (RT-qPCR). Total RNA was isolated using TRIZOL (Ambion; Thermo Fisher Scientific, Inc.). Afterwards, the RNA underwent phenol-chloroform extractions to further purify it. The quantity and quality (the acceptable ratio of A260/A280 was ≤1.8 and ≥2.2) of the purified RNA were assessed by measuring the absorbance at 260/280 nm (A_{260}/A_{280}) using Nanodrop One (NanoDrop Technologies; Thermo Fisher Scientific, Inc.). The level of gene expression was assessed using GAPDH as a control gene. cDNA synthesis [HiScript® III RT SuperMix for qPCR (+gDNA wiper), Vazyme Biotech Co., Ltd.] was performed using standard procedures (37˚C for 15 min, 85˚C for 5 sec, and then maintained at 4˚C) and RT-qPCR analysis was carried out on the Bio-Rad S1000 instrument with HieffÔ qPCR SYBR® Green Master Mix (Low Rox Plus) (Shanghai Yeasen Biotechnology Co., Ltd.). The procedure was as follows: 95˚C for 5 min, then 40 cycles at 95˚C for 10 sec, and 30 sec at 60˚C. Afterwards, the concentration of each transcript was normalized to the level of GAPDH mRNA using the $2^{-\Delta\Delta Cq}$ method (24). The primer sequences were as follows: GAPDH forward, 5'GGTCGGAGTCAACGGATTTG-3' and reverse, 5'-GGAAGATGGTGATGGGATTTC-3'; BCL2 forward, 5'-TCATGTGTGTGGAGAGCGTCAAC-3' and reverse, 5'-GTGTGCAGGTGCCGGTTCAG-3'; BIRC3 forward, 5'-TATCCACATCAGACAGCCCAGGAG-3' and reverse, 5'-TTCCACGGCAGCATTAATCACAGG-3'; AIFM1 forward, 5'-GGCGGCGGGTGCTTTGAAG-3' and reverse, 5'-CATGCCATCGCTGGAACAAGTTG-3'; IFNG forward, 5'-TGACTTGAATGTCCAACGCAAAGC-3' and reverse, 5'-CGACCTCGAAACAGCATCTGACTC-3'; and VDAC1 forward, 5'-GATTGACCCTGACGCCTGCTTC-3' and reverse, 5'-CTTGCCATCCAGAAGAGCTGACAG-3'.

Statistical analysis. All data calculation and statistical analysis were carried out by R software (https://www.r-project.

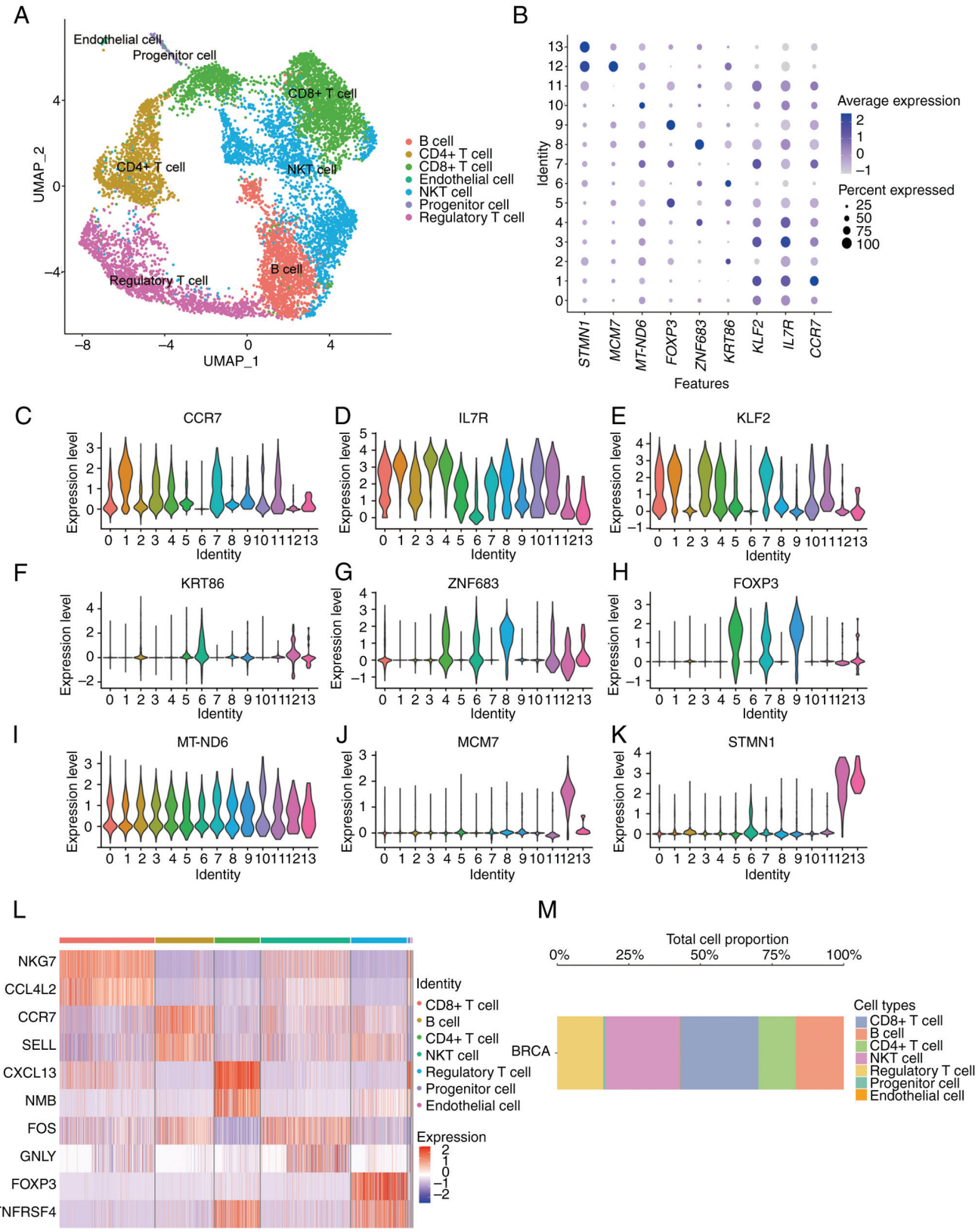

Figure 2. Cellular heterogeneity in single-cell data. (A) Uniform Manifold Approximation and Projection clustering diagram of 7 cells types in BC and normal samples. (B) The bubble diagram of marker genes' expression among different cell clusters (bubbles from small to large represent the proportion of gene expression in cell clusters from small to large, and the color from dark to light represents gene expression from strong to weak). (C-K) Violin plot of marker genes' expression among different cell clusters. (L) Heat map of differential genes (top10) among cell types (color from dark to light represents gene expression from strong to weak). (M) Proportion of each cell type in BC samples. BC, breast cancer.

org/; 4.1.2). For the comparison of two groups of continuous variables, the statistical significance of normal distribution variables was estimated by independent Student t-test, and the difference between non-normal distribution variables was

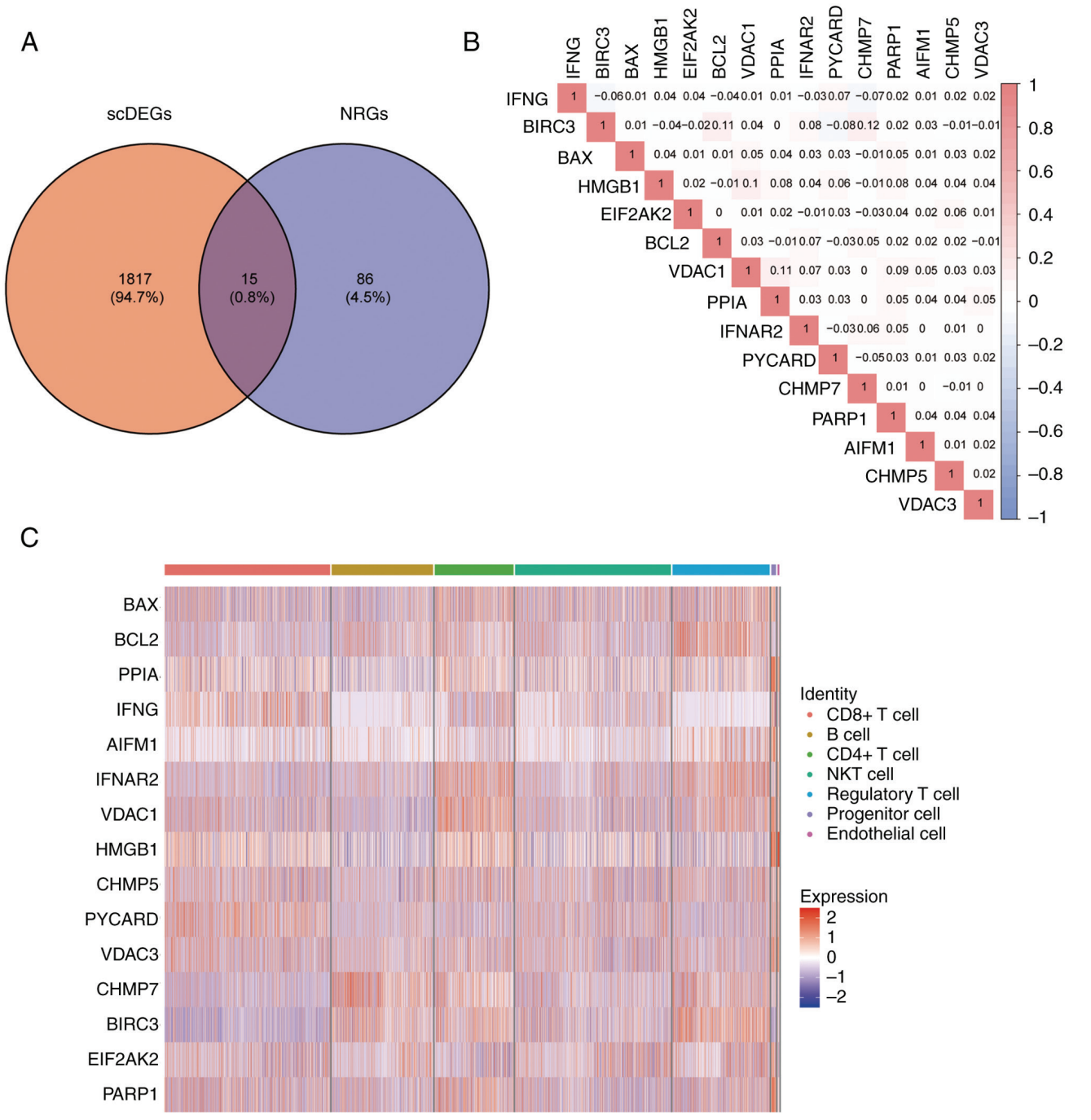

Figure 3. Correlation and differential analysis of key genes based on single-cell datasets. (A) A total of 15 key genes were obtained after the intersection of 1,832 single-cell differentially expressed genes and 101 necroptosis-related genes. (B) Heat map of correlation between key genes (red represents positive correlation, while blue represents negative correlation). (C) Heat map of expression of key genes in different cell types.

analyzed by Wilcoxon rank sum test. For the comparison of several groups of continuous variables, ANOVA (one-way, parametric) was used when the variance was uniform, and Kruskal-Wallis test (non-parametric) was used when the variance was uneven, and then Dunnett's was used for the appropriate multiple comparison test after the occurrence of significant results. The survival package of R was used for survival analysis, the Kaplan-Meier survival curve was used to show the difference in survival, and the log-rank test was used to evaluate the significant difference in survival time between the two groups. Univariate and multivariate Cox regression analysis was based on survival package, and LASSO model was based on 'glmnetR' package. All the statistical P-values were bilateral, and $P<0.05$ was considered to indicate a statistically significant difference.

Results

Cellular heterogeneity. The flow chart of the overall analysis of the present study is demonstrated in Fig. 1. The BC samples of single-cell data were integrated and CCA method was used to remove the batch effect, and then 'Seurat' package was used

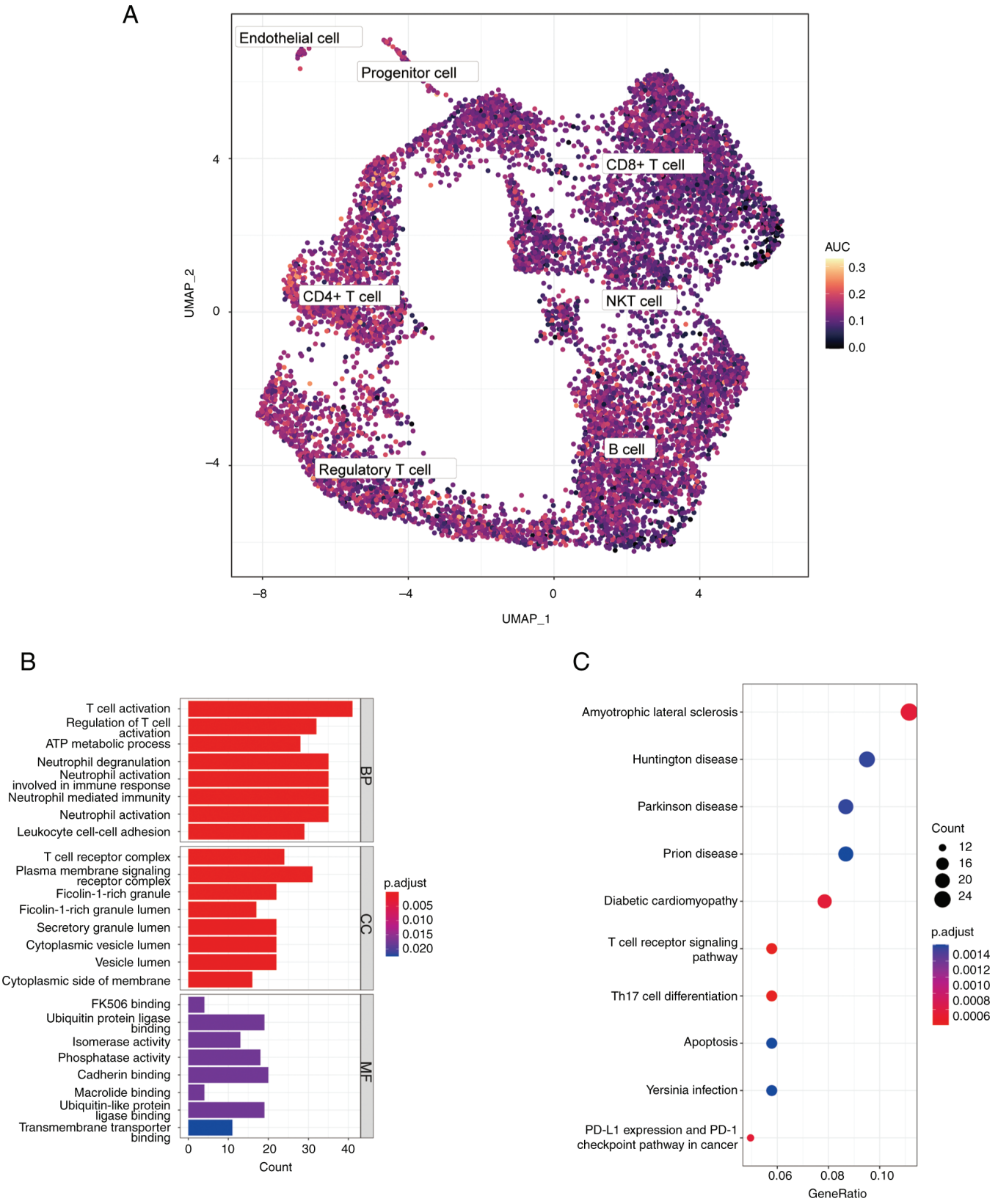

Figure 4. Activity AUCell score of key genes. (A) AUCell score Uniform Manifold Approximation and Projection map based on key genes in breast cancer single-cell data sets (color from black to red indicates score from low to high). (B) Enrichment of DEGs in biological process, cellular component and molecular function in Gene Ontology enrichment analysis. (C) Pathways enriched by DEGs in Kyoto Encyclopedia of Genes and Genomes pathway enrichment analysis. DEGs, differentially expressed genes.

to analyze the cellular heterogeneity of single-cell data. After removing the cells with mitochondrial gene content >5%, feature number <500 and UMI >20,000, the cluster diagrams of 7 cell types in BC samples were obtained by UMAP

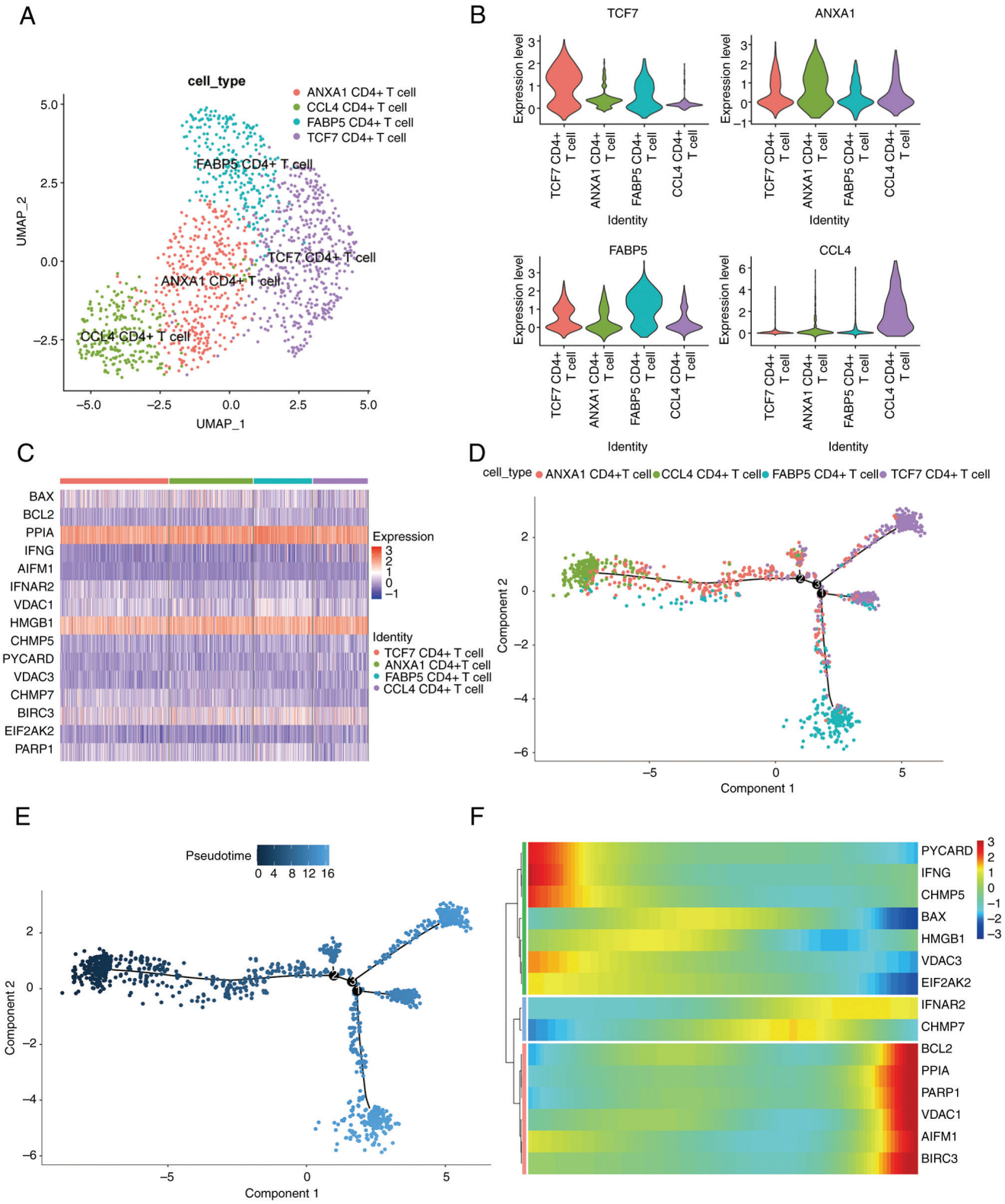

Figure 5. Analysis of new subtypes of CD4⁺ T cell clusters. (A) In total, 4 subtypes of CD4⁺ T cells were found by Uniform Manifold Approximation and Projection. (B) A total of 4 marker genes were highly expressed in their corresponding CD4⁺ T cell subtypes. (C) Heat map of the expression of key genes in the 4 CD4⁺ T cell subtypes (red indicates upregulated expression, while blue indicates downregulated expression). (D) CD4⁺ T cell subtype differentiation and development trajectory map (different colors represent different cell subtypes). (E) The sequence of differentiation and development of CD4⁺ T cell subtypes are CCL4 CD4⁺ T, ANXA1 CD4⁺ T, TCF7 CD4⁺ T and FASBP5 CD4⁺ T cells. (color from dark to light represents chronological order). (F) Pseudo-sequential dynamic heat map of key genes expressed in CD4⁺ T cell subtypes (red indicates upregulated expression, while blue indicates downregulated of expression).

clustering (Fig. 2A). Then the expression of marker genes in different cell clusters of 7 single-cell types was analyzed and shown by a bubble diagram (Fig. 2B). It was found that there were significant differences in marker genes' expression

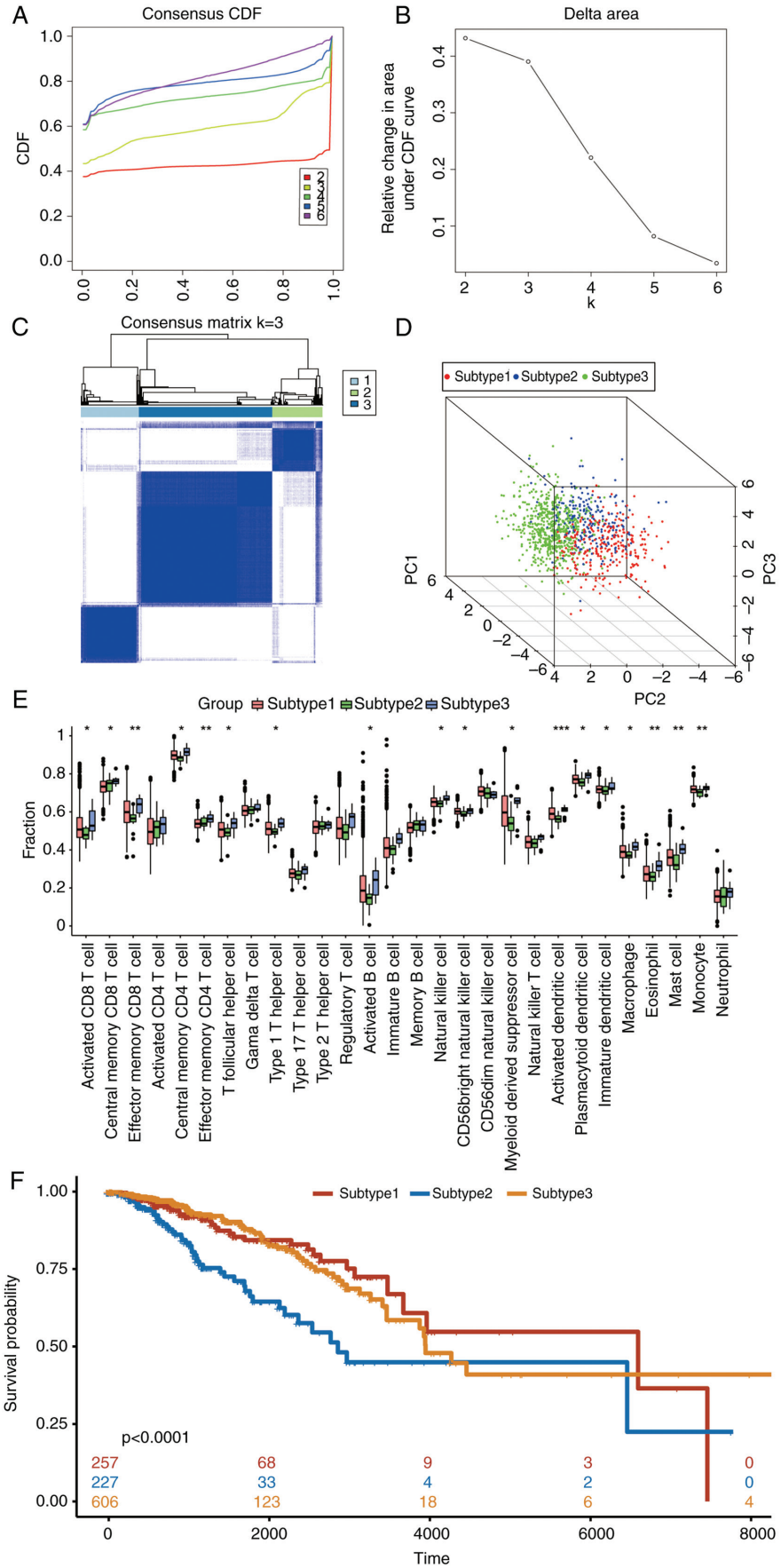

Figure 6. Identification of breast cancer molecular subtypes based on key genes. (A) CDF function graph during the clustering process. (B) CDF change diagram during the clustering process. (C) The result of clustering was selected as k=3, which is represented by the clustering heat map. (D) Principal component analysis showed that the 3 molecular subtypes of breast cancer could be well distinguished. *P<0.05, **P<0.01 and ***P<0.001. (E) Immune infiltration of different immune cells among 3 molecular subtypes of breast cancer. (F) Kaplan-Meier survival curve of 3 breast cancer subtypes. CDF, Cumulative distribution function

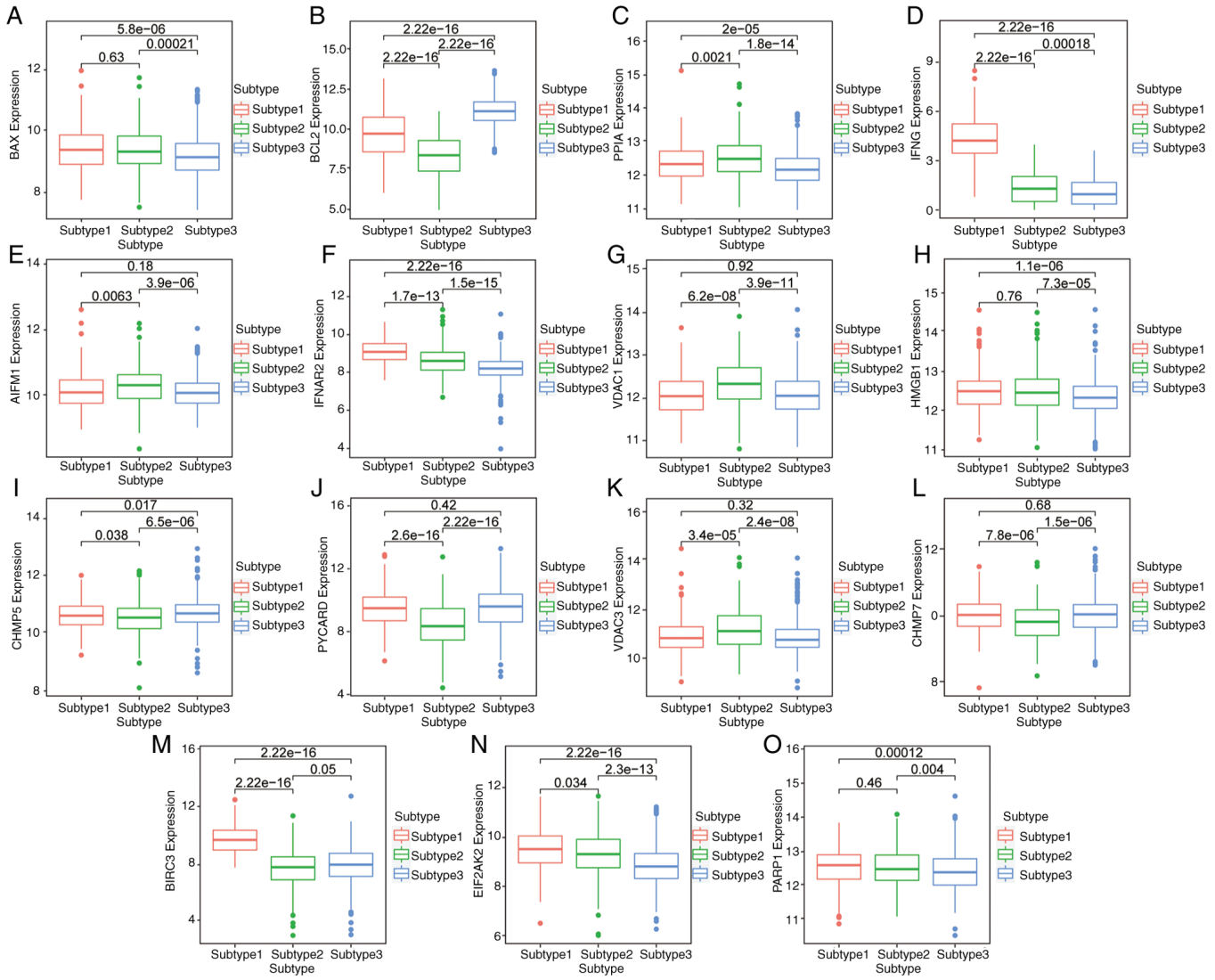

Figure 7. Differences in expression of key genes in breast cancer subtypes. (A) Compared with subtypes 1 and 2, the expression of BAX was lower in subtype 3. (B) The expression of BCL2 was different among the 3 subtypes, and its expression in subtype 3 was the highest. (C) The expression of PPIA was different among the 3 subtypes, and its expression in subtype 2 was the highest. (D) The expression level of IFNG in subtype 1 was significantly higher than that in subtypes 2 and 3. (E) Compared with subtypes 1 and 3, the expression of AIFM1 in subtype 2 was higher. (F) The expression of IFNAR2 in the 3 subtypes decreased in turn, and the difference was statistically significant. (G) VDAC1 was highly expressed in subtype 2. (H) The expression level of HMGB1 in subtype 3 was lower than that in subtypes 1 and 2. (I) CHMP5 was differentially expressed among the 3 subtypes, and its expression was the highest in subtype 3. (J) The expression of PYCARD in subtype 2 was reduced in a statistically significant manner. (K) The expression of VDAC3 in subtype 2 was significantly higher than that in subtypes 1 and 3. (L) The expression of CHMP7 in subtype 2 was significantly lower than that in subtypes 1 and 3. (M) BIRC3 was differentially expressed among the 3 subtypes, and the highest expression was found in subtype 1. (N) The expression level of EIF2AK2 in the 3 subtypes decreased in turn, which was statistically significant. (O) The expression level of PAR1 in subtype 3 was lower than that in subtypes 1 and 2.

among different cell clusters (Fig. 2C-K). At the same time, the expression differences among different cell populations were analyzed and the expression heat map of top 10 differential genes was constructed (Fig. 2L). Next, the differences in the proportion of different cell groups in patients with BC were also analyzed. It was found that CD8+ T cells accounted for the highest proportion in BC samples, followed by B cells and regulatory T cells, while progenitor cells accounted for the lowest, and other cell types had a similar proportion (Fig. 2M).

Analysis of correlation and difference of NRGs. For the seven cell types that had been annotated, the function 'FindAllMarkers' was used to calculate the differential genes among cell types, and a total of 1,832 scDEGs were selected based on |log2FoldChange|>0.25 and P<0.05. A total of 101 NRGs were obtained in the literature (18). Then, the intersection of NRGs and scDEGs was received (Fig. 3A) and 15 key genes resulted for follow-up research (BAX, BCL2, PPIA, IFNG, AIFM1, IFNAR2, VDAC1, HMGB1, CHMP5, PYCARD, VDAC3, CHMP7, BIRC3, EIF2AK2 and PARP1).

Through Pearson correlation analysis, it was found that there was a positive correlation in expression of most key genes, which indicated that there might be similar expression patterns of key genes in patients with BC (Fig. 3B). Among them, the correlation between CHMP7 and BIRC3 was the highest, while BIRC3 and PYCARD had the largest negative correlation. Finally, a heat map was used to demonstrate the expression of key genes in the cell populations (Fig. 3C).

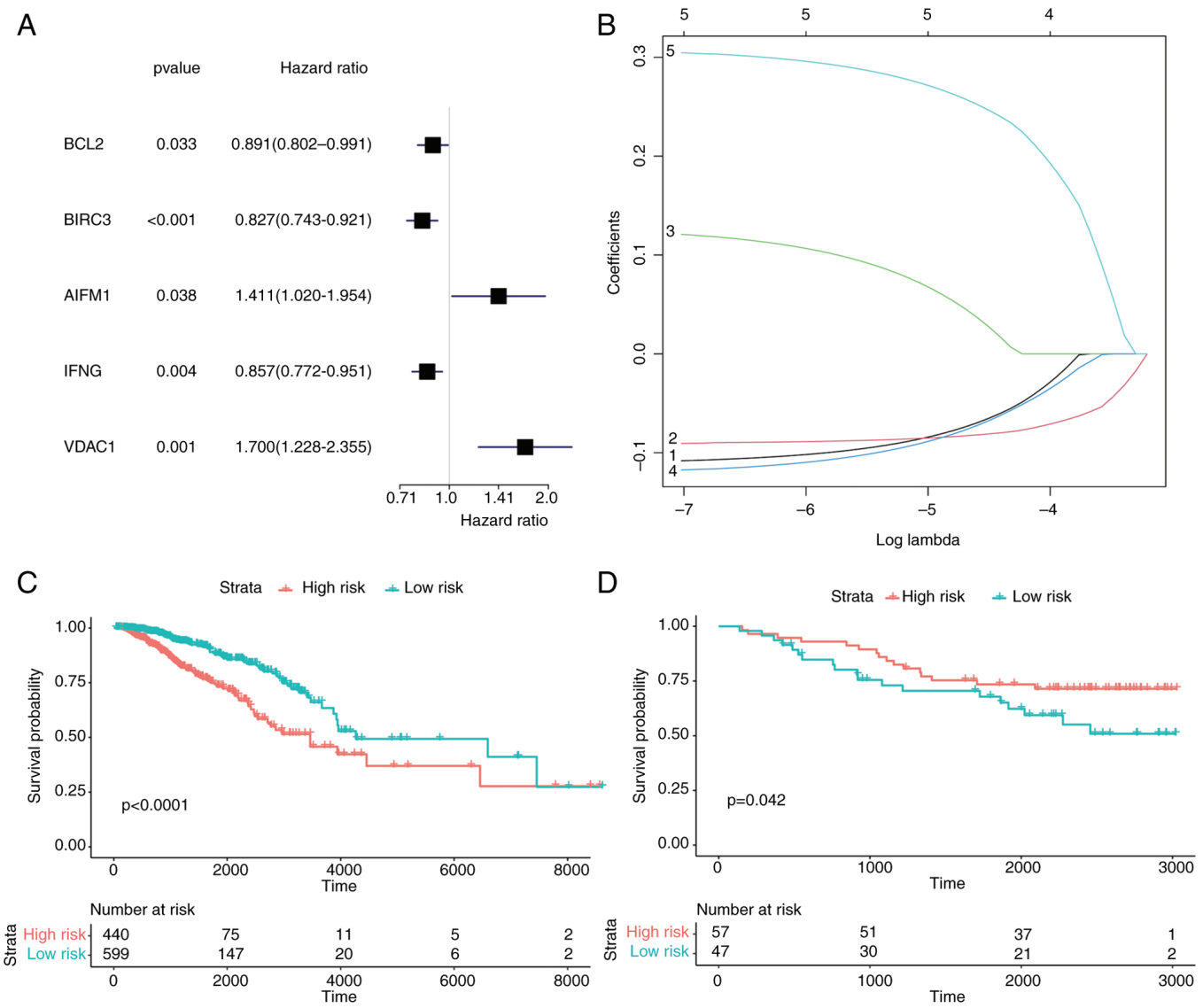

Figure 8. Construction of a prognostic risk model. (A) Univariate Cox regression analysis demonstrated that 5 genes, including BCL2, BIRC3, AIFM1, IFNG and VDAC1 were associated with the prognosis of patients with breast cancer. (B) Association between the selected features and the absolute value of the coefficient value. (C) In The Cancer Genome Atlas dataset, the survival rate of patients in the high-risk group was lower than that in the low-risk group. (D) Kaplan-Meier survival curve of the Least Absolute Shrinkage and Selection Operator Prognostic Model in the Gene Expression Omnibus dataset.

Key genes AUCell score. In order to verify the activity of key genes in different cell types, AUCell packages were used to demonstrate the activity of key genes in BC samples of single-cell data sets with UMAP maps (Fig. 4A). Through the UMAP map, it was found that CD4$^+$ T cells had higher AUCell scores, therefore CD4$^+$ T cells were defined as high-scoring cells with NRGs.

In order to explore whether there were significant differences in genes between high-scoring cell population and other cell populations, CD4$^+$ T cells were selected as a reference, using the function 'FindAllMarkers', and 499 DEGs were screened for GO and KEGG enrichment according to the standard of |log2FC|>0.5 and P<0.01. GO analysis revealed that DEGs were mainly related to T cell activation and regulation of T cell activation (Fig. 4B). KEGG analysis demonstrated that DEGs were related to T cell receptor signaling pathway, Th17 cell differentiation and PD-L1 expression and PD-1 checkpoint pathways in cancer (Fig. 4C). These results suggested that NRGs were highly active in CD4$^+$ T cells and might be involved in the activation of CD4$^+$ T cells.

Analysis of new subtypes of CD4$^+$ T cell cluster. In order to explore new subtypes of CD4$^+$ T cells, CD4$^+$ T cell clusters were clustered and four CD4$^+$ T cell subtypes were obtained, which were then annotated with significantly upregulated DEGs, resulting in ANXA1 CD4$^+$ T, CCL4 CD4$^+$ T, FASBP5 CD4$^+$ T and TCF7 CD4$^+$ T cells (Fig. 5A). For these four CD4$^+$ T cell subtypes, the function 'FindAllMarkers' was used to calculate the marker genes between them, and a violin map was employed to show the expression of marker genes in each subtype (Fig. 5B). To verify whether there was a difference in the expression of key genes among subsets of CD4$^+$ T cells, a heat was used map to demonstrate the results. It was found that there was no difference in the expression of the majority of key genes' subsets; only the expression of BAX2 was lower in CCL4 CD4$^+$ T cells (Fig. 5C). Subsequently, pseudotime

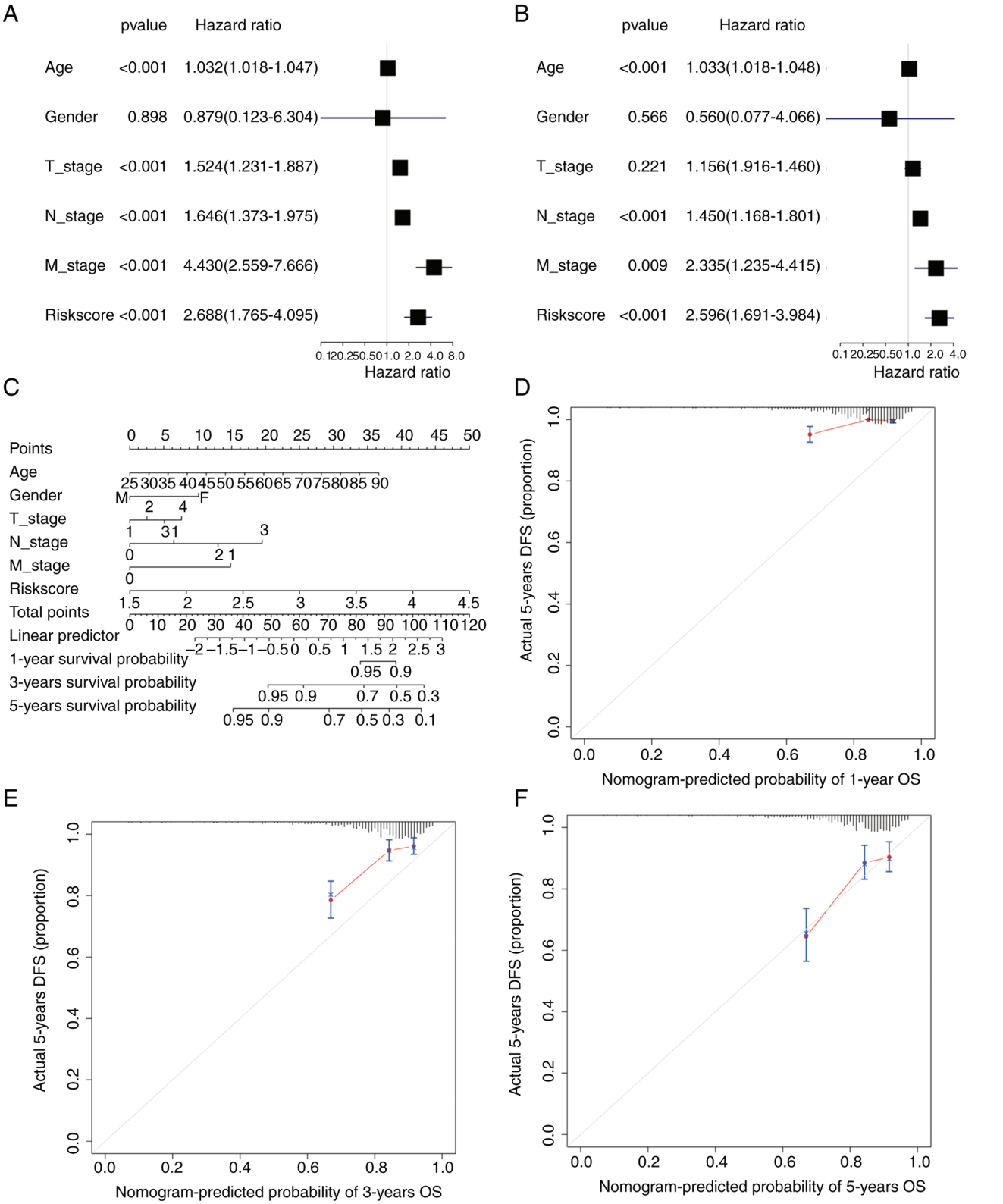

Figure 9. Constructing a nomogram and calibration curve for prognostic analysis of patients with BC based on the TCGA dataset. (A) Univariate Cox analysis showed that T-, N- and M-stage, and riskScore were risk factors for prognosis. (B) Multivariate Cox analysis showed that N- and M-stage, and riskScore were independent risk factors for prognosis. (C) Nomogram of clinical features. (D-F) Calibration curve at (D) 1, (E) 3 and (F) 5 years of the Cox regression model in TCGA-BC dataset. BC, breast cancer; TCGA, The Cancer Genome Atlas; OS, overall survival.

analysis was used to show the developmental trajectory of CD4$^+$ T cells, and the results revealed that the developmental trajectories among the subtypes were CCL4 CD4$^+$ T, ANXA1 CD4$^+$ T, TCF7 CD4$^+$ T and FASBP5 CD4$^+$ T cells (Fig. 5D and E). To analyze the changes in the expression of NRGs in the developmental trajectory, the expression of key genes was illustrated by heat maps (Fig. 5F). The expression of PYCARD, IFNG, CHMP5, BAX, HMGB1, VDAC3, EIF2AK2 and other

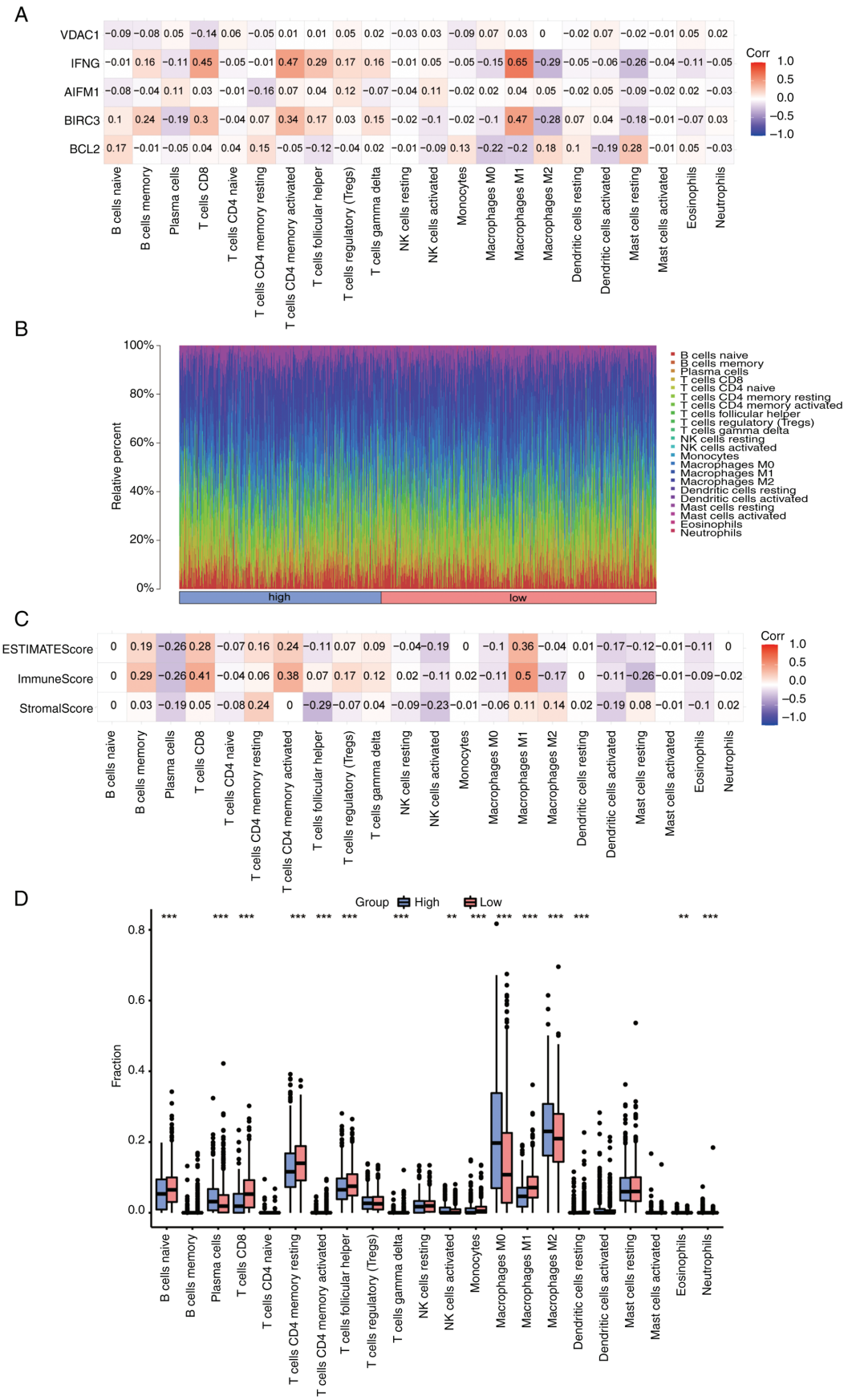

Figure 10. TCGA dataset Immune Infiltration Analysis of The Cancer Genome Atlas dataset. (A) Correlation analysis between prognosis genes (n=5) and immune cells (blue represents negative correlation, while red represents positive correlation, and the color from light to dark represents the correlation from weak to strong). (B) Panorama of infiltration of 22 immune cells types between BC high- and low-riskScore groups. (C) Correlation analysis between immune score and immune cells (blue represents negative correlation, while red represents positive correlation, and the color from light to dark represents the correlation from weak to strong). (D) Infiltration boxplot of 22 immune cells types between BC high- and low-riskScore groups. **P<0.01 and ***P<0.001. BC, breast cancer.

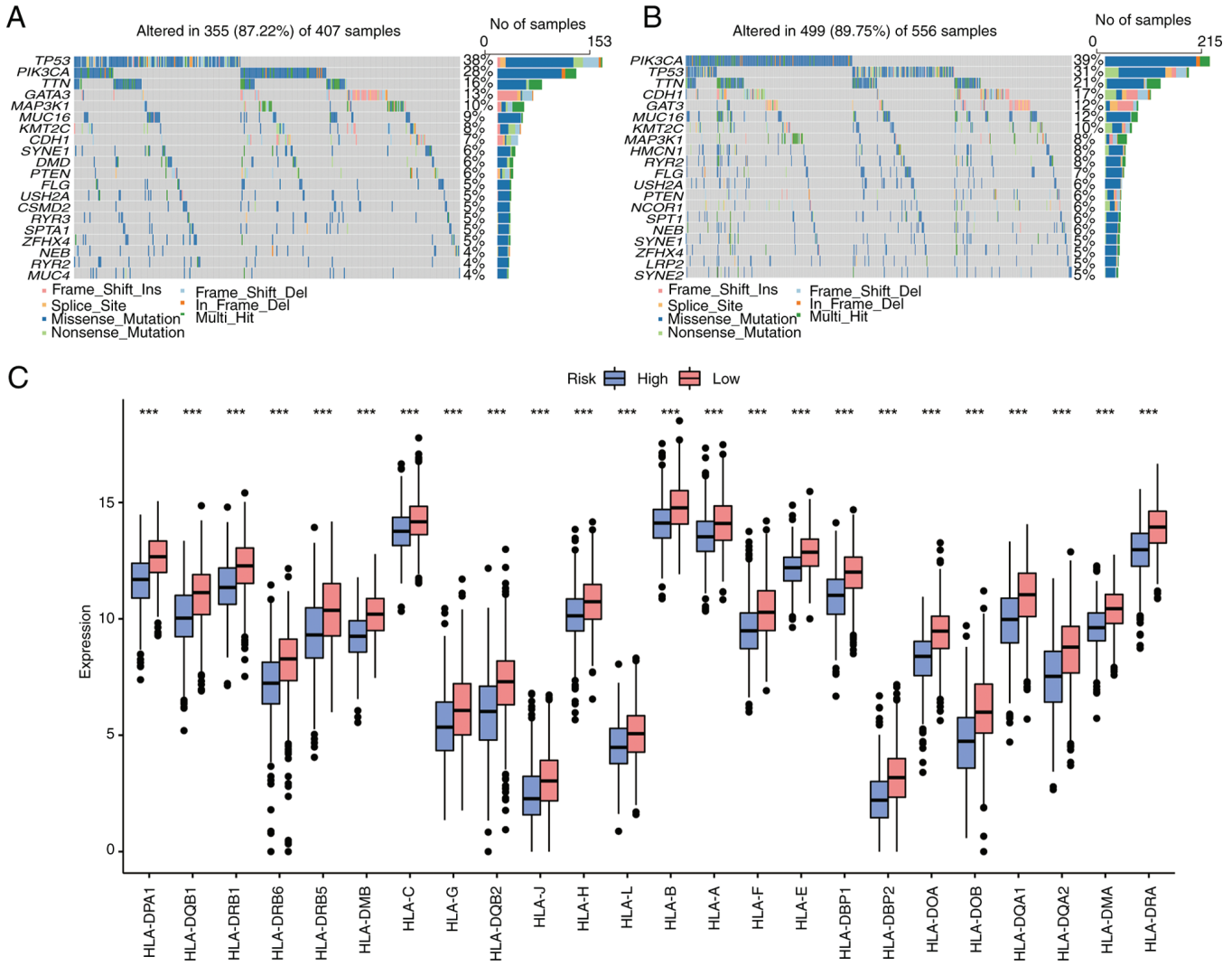

Figure 11. Mutation Analysis Based on somatic mutation dataset and The Cancer Genome Atlas datasets. (A) Top20 mutated genes in the high-risk group. (B) Top20 mutated genes in the low-risk group. (C) Boxplot of expression differences of human leukocyte antigen family genes between high- and low-riskScore groups. ***P<0.001.

genes was found to be downregulated during the development of CD4+ T cell subtypes, while the expression of BCL2, PPIA, PARP1, VDAC1, AIFM1, BIR3 and other genes was upregulated. This suggested that NRGs could regulate the development of CD4+ T cell subtypes.

Identification of BC molecular subtypes based on key genes. The aforementioned 15 key genes were employed as feature genes to carry out consistent clustering analysis of the samples in the TCGA-BC dataset. The process of selecting the k-value of the cluster is shown in Fig. 6A, and k=3 was selected as the result of clustering (Fig. 6B). The BC samples were divided into three disease subtypes: Subtype 1, 2 and 3. The clustering results were demonstrated by heat maps (Fig. 6C). PCA could distinguish different subtypes to a certain extent, indicating that there was a certain heterogeneity between different subtypes (Fig. 6D).

Single-sample Gene Set Enrichment Analysis was used to evaluate the differences in immune cells between BC molecular subtypes (Fig. 6E). The results revealed that the degree of immune cell infiltration in BC subtypes from high to low was subtypes 3, 1 and 2. Survival differences were then compared among the three molecular subtypes and illustrated with a KM survival curve (Fig. 6F). It was found that the survival rate of subtypes 1 and 3 was higher than that of subtype 2 (P<0.0001), which was consistent with a higher degree of immune cell infiltration and improved prognosis in these subtypes.

Differential expression of key genes in BC subtypes. The expression of key genes among different subtypes is shown with a box chart. The results identified that BAX, IFNG, IFNAR2, HMGB1, CHMP7, BIRC3, EIF2AK2 and PARP1 were most highly expressed in subtype 1 (Fig. 7A, D, F, H, L, M, N and O, respectively). The expression of PPIA, AIFM1, VDAC1 and VDAC3 was the highest in subtype 2 (Fig. 7C, E, G and K). BCL2, CHMP5 and PYCARD were most highly expressed in subtype 3 (Fig. 7B, I and J). This suggested that different subtypes could be distinguished by the expression level of key genes, and the prognosis of patients could be predicted.

Construction of a prognostic risk model based on key genes. To determine the prognostic genes of BC and analyze their diag-

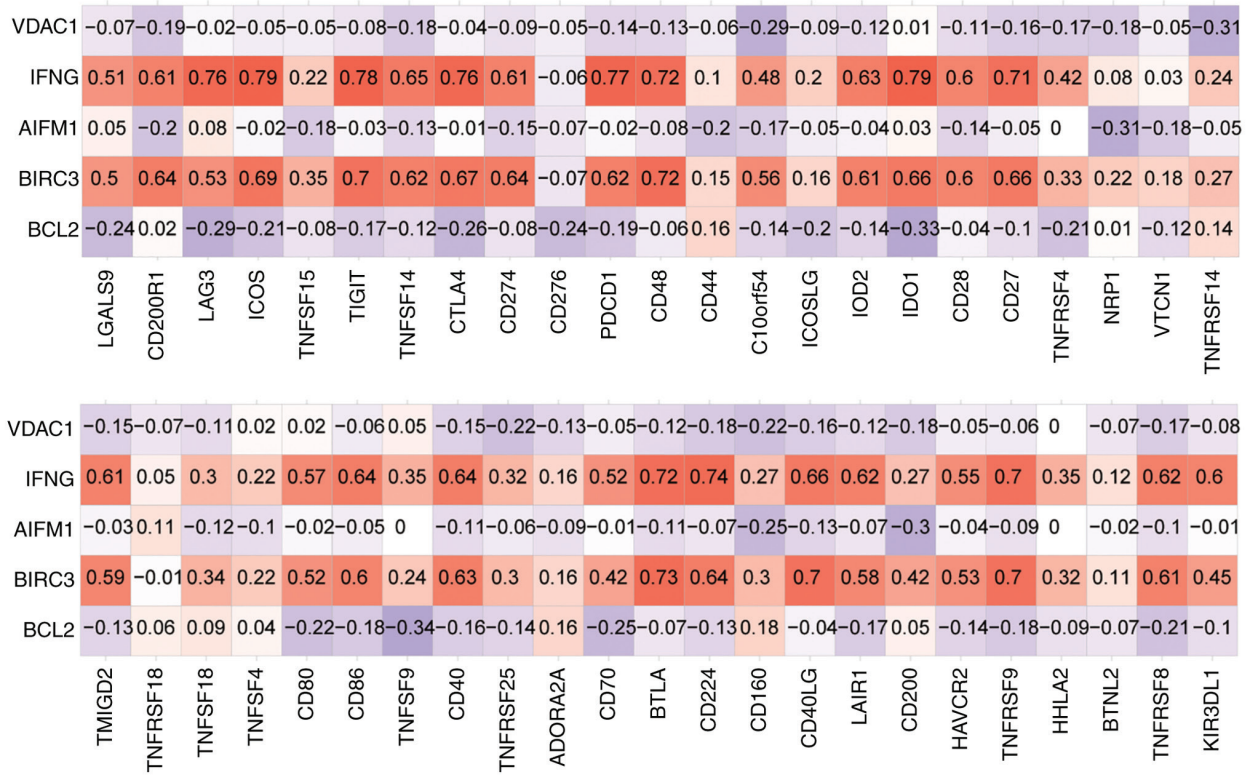

Figure 12. Correlation analysis of prognostic genes and immune checkpoints. Pearson correlation coefficient between prognostic genes and immune checkpoint genes.

nostic ability for diseases, based on 15 key genes (BAX, BCL2, PPIA, IFNG, AIFM1, IFNAR2, VDAC1, HMGB1, CHMP5, PYCARD, VDAC3, CHMP7, BIRC3, EIF2AK2 and PARP1), in the TCGA-BC datasets, univariate Cox regression analysis was first used to screen prognostic genes, and 5 genes were screened according to the criterion of P<0.05 (Fig. 8A). These 5 genes (BCL2, BIRC3, AIFM1, IFNG and VDAC1) in the model were identified as potential prognostic genes of BC by LASSO regression (Fig. 8B). According to the Cox risk regression coefficient of the 5 genes, the riskScores of each sample were calculated. The samples were divided into two groups by the cut-off provided by the R package 'maxstat', including 440 samples in the high-risk group and 599 samples in the low-risk group. According to the aforementioned grouping, survival analysis was conducted and a survival curve was drawn. In the LASSO prognostic model, the survival rate of the high-risk group was lower than that of the low-risk group (P<0.0001) (Fig. 8C).

Next, the prognosis model was validated with GEO datasets and a survival curve was generated through survival analysis. In contrast to the aforementioned results, the survival rate in the high-risk group was higher than that in the low-risk group (P<0.042) (Fig. 8D). This contradictory result may be caused by the heterogeneity between datasets and the differences in sample characteristics. Finally, the Receiver Operating Characteristic (ROC) curve was drawn and the AUC was calculated to verify the model. The results revealed that the AUC of TCGA-BC dataset was 0.595 (Fig. S1A), which had a certain prediction effect, while the AUC of GEO datasets was 0.457 (Fig. S1B), indicating that its prediction effect was poor.

Construction of a nomogram for patients with BC based on riskScores. Univariate and multivariate Cox regression analysis was performed based on the TCGA-BC dataset according to the patients' TNM stage, sex, age and riskScore. In univariate Cox regression, age, T-stage, N-stage, M-stage and riskScore had a significant influence on OS (P<0.001) (Fig. 9A), while only age, N-stage and riskScore had a significant effect in multivariate Cox regression (P<0.001) (Fig. 9B). A nomogram was also drawn using the 'rms' package (Fig. 9C). The 1-, 3- and 5-year survival probabilities of patients with BC were predicted by drawing 1- (Fig. 9D), 3- (Fig. 9E) and 5-year calibration curves (Fig. 9F). The results demonstrated that the 5-year nomogram model was the most consistent with the ideal model, and other nomogram models were essentially equal to the ideal model, indicating that the present model was relatively accurate.

Immune infiltration analysis. First, the correlation between 5 prognostic genes (BCL2, BIRC3, AIFM1, IFNG and VDAC1) and 22 types of immune cells was analyzed and visualized using CIBERSORT in the BC dataset (Fig. 10A). The positive correlation between IFNG and M1 macrophages was the highest (r=0.65, $P=1.6x10^{-125}$), while the negative correlation between IFNG and M2 macrophages was the highest (r=-0.29, $P=5.1x10^{-22}$). The infiltration panorama of 22 types of immune cells in each sample was next mapped (Fig. 10B). Finally, the ImmuneScore, StromalScore and EstimateScore in each sample were calculated by the ESTIMATE algorithm, and the correlation between each score and 22 types of immune cells was analyzed and visualized (Fig. 10C). The highest positive correlation was between ImmuneScore and M1 macrophages

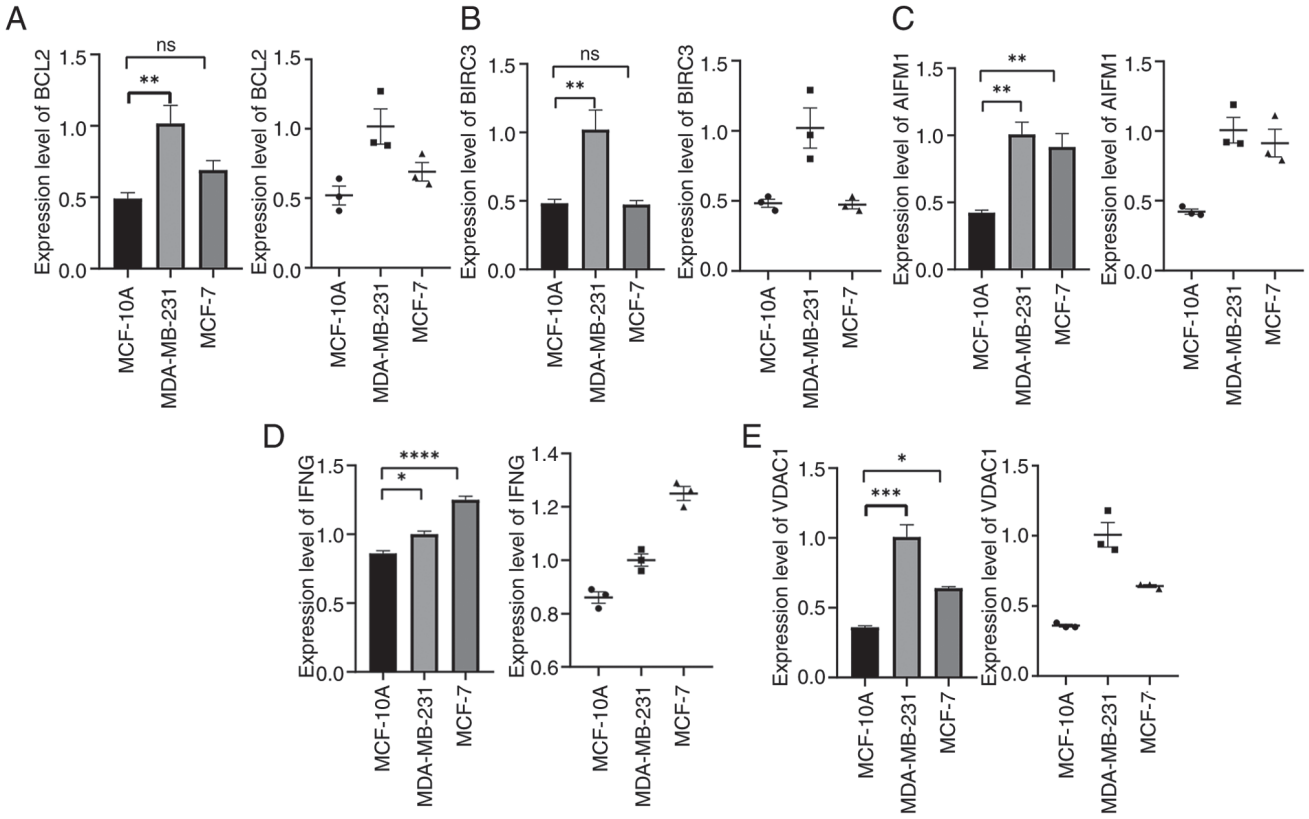

Figure 13. Verification of BCL2, BIRC3, AIFM1, IFNG, VDAC1 expression in MDA-MB-231, MCF-7 and MCF-10A cells. (A-E) mRNA expression level of (A) BCL2, (B) BIRC3, (C) AIFM1, (D) IFNG and (E) VDAC1 in MDA-MB-231, MCF-7 and MCF-10A cells. *P<0.05, **P<0.01, ***P<0.001 and ****P<0.0001. ns, not significant.

(r=0.5, P=7.7x10^{-66}). Finally, the differences in immune infiltration between high- and low-risk groups were shown as box plots (Fig. 10D). The results revealed that the infiltration of plasma cells, activated NK cells, M0 and M2 macrophages and eosinophils in the high-risk group was significantly higher than that in the low-risk group. However, compared with the high-risk group, the low-risk group had a higher degree of infiltration of naive B, CD8^{+} T cells, memory resting CD4^{+} T cells, memory activated CD4^{+} T cells and follicular helper T cells, as well as M1 macrophages and other immune cells.

Somatic mutation analysis and differential expression analysis of HLA family genes. According to the risk score of the aforementioned model, the total BC samples in the somatic mutation dataset were divided into high- and low-risk group, and the characteristics of various mutations in different groups were analyzed. The top 20 mutated genes in the high- and low-risk groups were analyzed (Fig. 11A and B), and it was found that there were differences in gene mutations in the two groups. The gene with the highest mutation frequency in the high-risk group was TP53, while in the low-risk group it was PIK3CA. The differential expression of HLA family genes in the high- and low-risk groups of TCGA-BC dataset was also analyzed. As revealed in Fig. 11C, various HLA molecules were upregulated in the low-risk group.

Correlation analysis of prognostic genes and immune checkpoints. The constructed LASSO model produced 5 BC prognostic genes (BCL2, BIRC3, AIFM1, IFNG and VDAC1), and 47 ICGs were obtained by consulting the literature (19). By calculating the Pearson correlation coefficient between the two, correlations of prognostic genes with immune checkpoints were obtained (Fig. 12). Among them, IFNG had the highest positive correlation with IDO1 and ICOS (r=0.79 and P=2.4x10^{-232}; r=0.79 and P=4.9x10^{-237}, respectively), while BCL2 had the highest negative correlation with TNFSF9 (r=0.34, P=1.3x10^{-30}).

Validation of the expression validation of prognostic genes. The mRNA expression of 5 prognostic genes (BCL2, BIRC3, AIFM1, IFNG and VDAC1) in the human BC cell lines MDA-MB-231 and MCF-7 and the human breast epithelial cell MCF-10A was detected by RT-qPCR. The results showed that, compared with MCF-10A, BCL2, BIRC3, AIFM1, IFNG and VDAC1 were significantly higher in the aforementioned BC cell lines (Fig. 13A-E) (P<0.05). Although the expression of BCL2 and BIRC3 in MCF-7 cells was higher than that in MCF-10A, there was no statistical significance (P>0.05). This suggested that the expression of BCL2 and BIRC3 genes may be related to BC types.

Discussion

It is well known that BC is a highly heterogeneous class of cancer, and the prognosis and treatment response of patients with different molecular characteristics vary greatly (25). Single-cell RNA-seq is an advanced method for studying the cellular heterogeneity of the TME in various cancer types (26). Necroptosis is involved in the immune response and TME, and the benefits of activation of necroptosis pathways combined with immune checkpoint

blockade have been demonstrated in a recent study (27). At present, the risk model of NRGs in BC and the potential ability to predict prognosis has not been elucidated at the single-cell level.

The present study identified a prognostic model containing 5 NRGs (BCL2, BIRC3, AIFM1, IFNG and VDAC1) at the single-cell level. Univariate Cox regression analysis showed that BCL2, BIRC3 and IFNG were protective factors, while AIFM1 and VDAC1 were risk factors. Among them, the BCL2 protein family could induce apoptosis and necroptosis (28). BCL2 is overexpressed in BC, and is an independent and powerful protein marker for favorable prognosis of early BC, which is not associated with time or adjuvant therapy (29). Therefore, BCL2 is the most potential therapeutic target. Currently, the mimic compound ABT-199 for BCL2, in combination with tamoxifen, showed a clinical benefit rate of 75% in a phase Ib/II clinical trial in ER^+ BC (30,31). BC is one of the tumor types where BIRC3 has not yet been fully characterized. In the majority of cases, BIRC3 is regarded as an oncogene with antiapoptotic functions; however, in BC, BIRC3 does not regulate any pathway of apoptosis (32). A recent study by Zhou *et al* (33) showed that BIRC3 was highly expressed in BC, and its high expression was associated with favorable prognosis. The dual function of BIRC3 may depend on the type of cancer and/or the molecular subtype of BC. Thus, this gene needs to be further studied to clarify its role in BC. IFNG is the only type II IFN cytokine that can induce necroptosis by activating RIP1 serine-threonine kinase to exert antitumor effects (34). Previous studies have revealed that high expression of IFNG has a survival advantage over low expression in patients with BC and cervical cancer (35,36), which shows that IFNG is a protective factor, which is consistent with the results of the present study. AIFM1 is not only a risk gene for the prognosis of BC, but also promotes the occurrence of cervical cancer (37,38). This suggests that inhibiting the expression of AIFM1 is beneficial to the prognosis of patients with BC. Fang *et al* (39) reported that overexpressed VDAC1 in BC could be used as a new biomarker for diagnosis. VDAC1 is an independent factor for predicting poor prognosis. VDAC1 may inhibit tumor immunity and may be a new therapeutic target for BC. Compared with the prediction ability of a single gene, the comprehensive prediction efficiency of 5 genes for BC is higher. As a result, the combination of these genes may have an unexpected effect in optimizing the prognostic assessment strategy of BC.

Necroptosis participates in the immune response in two ways: On one hand, tumor cells release damage-associated molecular patterns to dendritic cells after necroptosis to trigger antigen presentation and activate $CD8^+$ T cells (27). On the other hand, it has been reported that RIPK1 and RIPK3 can directly regulate the function of NK cells independently of the necroptosis pathway, and play a role in promoting antitumor immune responses (40). The present study showed that NRGs were highly active in $CD4^+$ T cells and differentially expressed in the developmental trajectory of the four subtypes of cells. This suggests that NRGs may be involved in the differentiation and development of $CD4^+$ T cells, thus affecting the function of $CD4^+$ T cells. Kwok *et al* (41) identified that necroptosis was involved in $CD4^+$ T cell-mediated microvascular endothelial cell death and chronic cardiac allograft rejection. In cancer, there is a lack of research on necroptosis and $CD4^+$ T cells. Furthermore, in addition to M1 macrophages, activated $CD4^+$ T cells had the highest immuneScore. This indicated that $CD4^+$ T cells have more immune components and can play an important role in immunotherapy. The present results suggested that NRGs may become an effective molecule to improve the antitumor immune function of $CD4^+$ T cells; however, further research is still needed to confirm.

Immune infiltration in the TME has an important influence on the clinical features and prognosis of BC (42). The current study was divided into high- and low-risk groups according to the median risk score, and the results suggested that immune cell infiltration in the low-risk group was higher than that in the high-risk group. Patients in the low-risk group had a higher OS than those in the high-risk group. In BC, high immune infiltration has been associated with improved clinical outcome (43), which is consistent with the present findings. Groups with high immune infiltration may benefit to a greater extent from immunotherapy (44). This suggests that patients in the low-risk group are more sensitive to immunotherapy. In addition, 5 prognostic genes were correlated with multiple immune checkpoints such as IDO1 which may lead to new targets for BC immunotherapy.

The present study has several limitations, including: i) The differentiation role of NRGs in $CD4^+$ T cells requires further experimental research, which will be the authors' next research plan; ii) it lacks mechanism and animal experiments to verify the regulatory mechanism of necrotizing apoptosis-related genes in BC, which will be further explored in the future; iii) there is insufficient number of patients in the external clinical cohort, and large-scale clinical trials are therefore required to verify the accuracy of the results; and iv) there are multiple datasets, which may cause inter-batch differences that cannot be avoided and removed during analysis.

In conclusion, the present study successfully established an NRG signature based on BCL2, BIRC3, AIFM1, IFNG and VDAC1 at the single-cell level, and explored the association between risk model and immune infiltration. Secondly, the current study found that NRGs were involved in the differentiation and development of $CD4^+$ T cells. These findings pointed novel ways of BC prognosis estimation and potential immunotherapy strategies.

Acknowledgements

Not applicable.

Funding

The present study was supported by the National Natural Science Foundation of China (grant no. 82060479) and the Key Research and Development Project of Ningxia Hui Autonomous Region (grant no. 2021BEG03062).

Availability of data and materials

The data generated in the present study may be found in The Cancer Genome Atlas (https://portal.gdc.cancer.gov/projects/TCGA-BRCA) and Gene Expression Omnibus databases under accession numbers GSE114724 and

GSE42568 or at the following URL: https://www.ncbi.nlm.nih.gov/gds/?term=GSE114724 and https://www.ncbi.nlm.nih.gov/gds/?term=GSE114724.

Authors' contributions

JL designed the study. JL and LG confirm the authenticity of all the raw data. LG and XM performed data analysis and drafted the manuscript. HL and SY performed verification experiments and improved the language of the manuscript. KZ downloaded the raw data and modified the manuscript with JL. All authors read and approved the final manuscript.

Ethics approval and consent to participate

Not applicable.

Patient consent for publication

Not applicable.

Competing interests

The authors declare that they have no competing interests.

References

1. Loibl S, Poortmans P, Morrow M, Denkert C and Curigliano G: Breast cancer. Lancet 397: 1750-1769, 2021.
2. Zhou J, Su CM, Chen HA, Du S, Li CW, Wu H, Tsai SH and Yeh YT: Cryptanshinone inhibits the glycolysis and inhibits cell migration through PKM2/β-catenin axis in breast cancer. Onco Targets Ther 13: 8629-8639, 2020.
3. Mao YJ, Lim HJ, Ni M, Yan WH, Wong DW and Cheung JC: Breast tumour classification using ultrasound elastography with machine learning: A systematic scoping review. Cancers (Basel) 14: 367, 2022.
4. Yankaskas CL, Thompson KN, Paul CD, Vitolo MI, Mistriotis P, Mahendra A, Bajpai VK, Shea DJ, Manto KM, Chai AC, *et al*: A microfluidic assay for the quantification of the metastatic propensity of breast cancer specimens. Nat Biomed Eng 3: 452-465, 2019.
5. Roychowdhury S, McCullough RL, Sanz-Garcia C, Saikia P, Alkhouri N, Matloob A, Pollard KA, McMullen MR, Croniger CM and Nagy LE: Receptor interacting protein 3 protects mice from high-fat diet-induced liver injury. Hepatology 64: 1518-1533, 2016.
6. Kaczmarek A, Vandenabeele P and Krysko DV: Necroptosis: The release of damage-associated molecular patterns and its physiological relevance. Immunity 38: 209-223, 2013.
7. Gong Y, Fan Z, Luo G, Yang C, Huang Q, Fan K, Cheng H, Jin K, Ni Q, Yu X and Liu C: The role of necroptosis in cancer biology and therapy. Mol Cancer 18: 100, 2019.
8. Daniels BP, Kofman SB, Smith JR, Norris GT, Snyder AG, Kolb JP, Gao X, Locasale JW, Martinez J, Gale M Jr, *et al*: The nucleotide sensor ZBP1 and kinase RIPK3 induce the enzyme iRG1 to promote an antiviral metabolic state in neurons. Immunity 50: 64-76.e4, 2019.
9. Park JE, Lee JH, Lee SY, Hong MJ, Choi JE, Park S, Jeong JY, Lee EB, Choi SH, Lee YH, *et al*: Expression of key regulatory genes in necroptosis and its effect on the prognosis in non-small cell lung cancer. J Cancer 11: 5503-5510, 2020.
10. Li X, Guo J, Ding AP, Qi WW, Zhang PH, Lv J, Qiu WS and Sun ZQ: Association of mixed lineage kinase domain-like protein expression with prognosis in patients with colon cancer. Technol Cancer Res Treat 16: 428-434, 2017.
11. Höckendorf U, Yabal M, Herold T, Munkhbaatar E, Rott S, Jilg S, Kauschinger J, Magnani G, Reisinger F, Heuser M, *et al*: RIPK3 restricts myeloid leukemogenesis by promoting cell death and differentiation of leukemia initiating cells. Cancer Cell 30: 75-91, 2016.
12. Jiao D, Cai Z, Choksi S, Ma D, Choe M, Kwon HJ, Baik JY, Rowan BG, Liu C and Liu ZG: Necroptosis of tumor cells leads to tumor necrosis and promotes tumor metastasis. Cell Res 28: 868-870, 2018.
13. He X, Feng Z, Ma J, Ling S, Cao Y, Gurung B, Wu Y, Katona BW, O'Dwyer KP, Siegel DL, *et al*: Bispecific and split CAR T cells targeting CD13 and TIM3 eradicate acute myeloid leukemia. Blood 135: 713-723, 2020.
14. Wu Y, Kyle-Cezar F, Woolf RT, Naceur-Lombardelli C, Owen J, Biswas D, Lorenc A, Vantourout P, Gazinska P, Grigoriadis A, *et al*: An innate-like Vδ1^{+} γδ T cell compartment in the human breast is associated with remission in triple-negative breast cancer. Sci Transl Med 11: eaax9364, 2019.
15. Snyder AG, Hubbard NW, Messmer MN, Kofman SB, Hagan CE, Orozco SL, Chiang K, Daniels BP, Baker D and Oberst A: Intratumoral activation of the necroptotic pathway components RIPK1 and RIPK3 potentiates antitumor immunity. Sci Immunol 4: eaaw2004, 2019.
16. Chung W, Eum HH, Lee HO, Lee KM, Lee HB, Kim KT, Ryu HS, Kim S, Lee JE, Park YH, *et al*: Single-cell RNA-seq enables comprehensive tumour and immune cell profiling in primary breast cancer. Nat Commun 8: 15081, 2017.
17. Zou Y, Ye F, Kong Y, Hu X, Deng X, Xie J, Song C, Ou X, Wu S and Wu L: The single-cell landscape of intratumoral heterogeneity and the immunosuppressive microenvironment in liver and brain metastases of breast cancer. Adv Sci (Weinh) 10: e2203699, 2023.
18. Fu X, Wu X, Djekidel MN and Zhang Y: Myc and Dnmt1 impede the pluripotent to totipotent state transition in embryonic stem cells. Nat Cell Biol 21: 835-844, 2019.
19. Shigemizu D, Iwase T, Yoshimoto M, Suzuki Y, Miya F, Boroevich KA, Katagiri T, Zembutsu H and Tsunoda T: The prediction models for postoperative overall survival and disease-free survival in patients with breast cancer. Cancer Med 6: 1627-1638, 2017.
20. Feng H, Zhong L, Yang X, Wan Q, Pei X and Wang J: Development and validation of prognostic index based on autophagy-related genes in patient with head and neck squamous cell carcinoma. Cell Death Discov 6: 59, 2020.
21. Xu D, Liu X, Wang Y, Zhou K, Wu J, Chen JC, Chen C, Chen L and Zheng J: Identification of immune subtypes and prognosis of hepatocellular carcinoma based on immune checkpoint gene expression profile. Biomed Pharmacother 126: 109903, 2020.
22. Liu D, Schilling B, Liu D, Sucker A, Livingstone E, Jerby-Arnon L, Zimmer L, Gutzmer R, Satzger I, Loquai C, *et al*: Integrative molecular and clinical modeling of clinical outcomes to PD1 blockade in patients with metastatic melanoma. Nat Med 25: 1916-1927, 2019.
23. Ru B, Wong CN, Tong Y, Zhong JY, Zhong SSW, Wu WC, Chu KC, Wong CY, Lau CY, Chen I, *et al*: TISIDB: An integrated repository portal for tumor-immune system interactions. Bioinformatics 35: 4200-4202, 2019.
24. Livak KJ and Schmittgen TD: Analysis of relative gene expression data using real-time quantitative PCR and the 2(-Delta Delta C(T)) method. Methods 25: 402-408, 2001.
25. Nguyen VC, Nguyen TQ, Vu TNH, Phung TH, Nguyen TPH, Nguyen ND and Le DR: Application of St Gallen categories in predicting survival for patients with breast cancer in Vietnam. Cancer Control 26: 1073274819862794, 2019.
26. Xie J, Deng W, Deng X, Liang JY, Tang Y, Huang J, Tang H, Zou Y, Zhou H and Xie X: Single-cell histone chaperones patterns guide intercellular communication of tumor microenvironment that contribute to breast cancer metastases. Cancer Cell Int 23: 311, 2023.
27. Gao W, Wang X, Zhou Y, Wang X and Yu Y: Autophagy, ferroptosis, pyroptosis, and necroptosis in tumor immunotherapy. Signal Transduct Target Ther 7: 196, 2022.
28. Li X, Chen M, Shi Q, Zhang H and Xu S: Hydrogen sulfide exposure induces apoptosis and necroptosis through lncRNA3037/miR-15a/BCL2-A20 signaling in broiler trachea. Sci Total Environ 699: 134296, 2020.
29. Dawson SJ, Makretsov N, Blows FM, Driver KE, Provenzano E, Le Quesne J, Baglietto L, Severi G, Giles GG, McLean CA, *et al*: BCL2 in breast cancer: A favourable prognostic marker across molecular subtypes and independent of adjuvant therapy received. Br J Cancer 103: 668-675, 2010.
30. Zhang L, Lu Z and Zhao X: Targeting Bcl-2 for cancer therapy. Biochim Biophys Acta Rev Cancer 1876: 188569, 2021.
31. Lok SW, Whittle JR, Vaillant F, Teh CE, Lo LL, Policheni AN, Bergin ART, Desai J, Ftouni S, Gandolfo LC, *et al*: A phase Ib dose-escalation and expansion study of the BCL2 inhibitor venetoclax combined with tamoxifen in ER and BCL2-positive metastatic breast cancer. Cancer Discov 9: 354-369, 2019.

32. Frazzi R: BIRC3 and BIRC5: Multi-faceted inhibitors in cancer. Cell Biosci 11: 8, 2021.
33. Zhou Q, Xu Y, Shen L, Yang X and Wang L: Identification of a novel necroptosis-related classifier to predict prognosis and guide immunotherapy in breast invasive carcinoma. Front Oncol 12: 852365, 2022.
34. Zaidi MR: The interferon-gamma paradox in cancer. J Interferon Cytokine Res 39: 30-38, 2019.
35. Wu ZH, Tang Y, Yu H and Li HD: The role of ferroptosis in breast cancer patients: A comprehensive analysis. Cell Death Discov 7: 93, 2021.
36. Rotman J, den Otter LAS, Bleeker MCG, Samuels SS, Heeren AM, Roemer MGM, Kenter GG, Zijlmans HJMAA, van Trommel NE, de Gruijl TD and Jordanova ES: PD-L1 and PD-L2 expression in cervical cancer: Regulation and biomarker potential. Front Immunol 11: 596825, 2020.
37. Zou R, Zhao W, Xiao S and Lu Y: A signature of three apoptosis-related genes predicts overall survival in breast cancer. Front Surg 9: 863035, 2022.
38. Zhang Y, Yang Y, Liu R, Meng Y, Tian G and Cao Q: Downregulation of microRNA-425-5p suppresses cervical cancer tumorigenesis by targeting AIFM1. Exp Ther Med 17: 4032-4038, 2019.
39. Fang Y, Liu J, Zhang Q, She C, Zheng R, Zhang R, Chen Z, Chen C and Wu J: Overexpressed VDAC1 in breast cancer as a novel prognostic biomarker and correlates with immune infiltrates. World J Surg Oncol 20: 211, 2022.
40. Liu Z and Chan FK: Regulatory mechanisms of RIPK1 in cell death and inflammation. Semin Cell Dev Biol 109: 70-75, 2021.
41. Kwok C, Pavlosky A, Lian D, Jiang J, Huang X, Yin Z, Liu W, Haig A, Jevnikar AM and Zhang ZX: Necroptosis is involved in CD4+ T cell-mediated microvascular endothelial cell death and chronic cardiac allograft rejection. Transplantation 101: 2026-2037, 2017.
42. Zhang Z, Li J, He T and Ding J: Bioinformatics identified 17 immune genes as prognostic biomarkers for breast cancer: Application study based on artificial intelligence algorithms. Front Oncol 10: 330, 2020.
43. Tekpli X, Lien T, Røssevold AH, Nebdal D, Borgen E, Ohnstad HO, Kyte JA, Vallon-Christersson J, Fongaard M, Due EU, *et al*: An independent poor-prognosis subtype of breast cancer defined by a distinct tumor immune microenvironment. Nat Commun 10: 5499, 2019.
44. Shi W, Chen Z, Liu H, Miao C, Feng R, Wang G, Chen G, Chen Z, Fan P, Pang W and Li C: COL11A1 as an novel biomarker for breast cancer with machine learning and immunohistochemistry validation. Front Immunol 13: 937125, 2022.